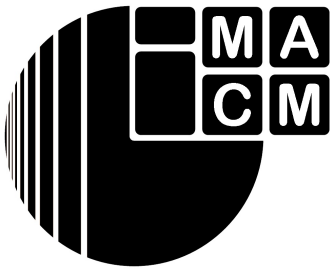

Bergische Universität Wuppertal

Fachbereich Mathematik und Naturwissenschaften

Institute of Mathematical Modelling, Analysis and Computational Mathematics (IMACM)

Preprint BUW-IMACM 20/09

A. Liefke, P. Jaksch, S. Schmitz, V. Marciniak, U. Janoske and H. Gottschalk

TOWARDS MULTIDISCIPLINARY TURBINE BLADE TOLERANCE DESIGN ASSESSMENT USING ADJOINT METHODS

April 25, 2020

http://www.math.uni-wuppertal.de

Proceedings of ASME Turbo Expo 2020
Turbomachinery Technical Conference and Exposition
GT2020
June 22-26, 2020, London, UK

GT2020-14501

TOWARDS MULTIDISCIPLINARY TURBINE BLADE TOLERANCE DESIGN ASSESSMENT USING ADJOINT METHODS

Alexander Liefke*
Siemens AG, Gas and Power
Mülheim an der Ruhr
45473, Germany
alexander.liefke@siemens.com

Peter Jaksch
Siemens Industrial Turbomachinery
Finspång
Sweden
peter.jaksch@siemens.com

Sebastian Schmitz
Siemens AG, Gas and Power
10553, Berlin
Germany
schmitz.sebastian@siemens.com

Vincent Marciniak
Siemens AG, Gas and Power
Mülheim an der Ruhr
45473, Germany
vincent.marciniak@siemens.com

Uwe Janoske
Chair of Fluid Mechanics
University of Wuppertal
Wuppertal, 42119, Germany
uwe.janoske@uni-wuppertal.de

Hanno Gottschalk
School of Mathematics and Science
University of Wuppertal
Wuppertal, 42119, Germany
hanno.gottschalk@uni-wuppertal.de

ABSTRACT

This paper shows how to use discrete CFD and FEM adjoint surface sensitivities to derive objective-based tolerances for turbine blades, instead of relying on geometric tolerances. For this purpose a multidisciplinary adjoint evaluation tool chain is introduced to quantify the effect of real manufacturing imperfections on aerodynamic efficiency and probabilistic low cycle fatigue life time.

Before the adjoint method is applied, a numerical validation of the CFD and FEM adjoint gradients is performed using 102 heavy duty turbine vane scans. The results show that the absolute error for adjoint CFD gradients is below 0.5%, while the FEM life time gradient absolute errors are below 5%. The adjoint assessment tool chain further reduces the computational cost by around 85% for the investigated test case compared to non-linear methods.

Through the application of the presented tool chain, the definition of specified objective-based tolerances becomes available as a design assessment tool and allows to improve overall turbine efficiency and the accuracy of life time prediction.

NOMENCLATURE

AD	Algorithmic differentiation
BC	Bond Coating
CFD	Computational Fluid Dynamics
CMB	Coffin-Manson-Basquin
FD	Finite Difference
FEM	Finite Element Method
E	Young Modulus
H	Total Enthalpy
J	Objective Function
K	Stiffness Matrix
L	Lagrange Function
LCF	Low Cycle Fatigue
RANS	Reynolds Averaged Navier Stokes
TBC	Thermal Barrier Coating
TMF	Thermo Mechanical Fatigue

*Address all correspondence to this author.

X	Node Coordinates
b	Fatigue Strength Exponent
c	Fatigue Ductility Exponent
$\bar{f}$	Load Vector
m	Weibull Shape Parameter for LCF
n	Number of Cycles
N_i	Load cycles until crack initiation
$\bar{u}$	Node Displacement
x_i	Node Variation in Normal Direction
η_{is}	Isentropic Efficiency
η_{LCF}	Weibull Scale Parameter for LCF
$\bar{\lambda}$	Adjoint / Lagrange Operator
$\partial\Omega$	2D Domain Surface
μ	Arithmetic Average
σ	Standard Deviation
σ_{VM}	Von Mises Stresses
σ'_f	Fatigue Strength Coefficient
ε'_f	Fatigue Ductility Coefficient

INTRODUCTION

Turbine blade geometric tolerances are usually based on engineering experience, manufacturability and product cost. A predefined number of points are measured on the blade surface to verify that the manufactured blades are within the specified tolerance range, which is typically below 1mm as shown by Liu et al. [1].

These geometric tolerances for blade surface areas, however, are an unnecessary intermediary step. The geometric-based tolerances decouple the original component design objectives e.g. efficiency and life time, using geometric dimensions to retrieve a measurable quality criteria for manufacturing. In an effort to improve these geometric tolerance ranges, a publication by Dow and Wang [2] optimized a 2D compressor blade introducing geometric tolerance bands, continuing the decoupling process.

So far geometric tolerances are deemed necessary, due to the lack of fast computational evaluation tools to analyze the impact of manufacturing imperfections. One possible solution for this are surrogate models as shown by Nigro et al. [3] for a compressor blade uncertainty quantification study. Another approach is the adjoint method.

The adjoint method allows to quantify the impact of numerous blade geometries for a given set of objectives through a simple multiplication, instead of multiple computational expensive RANS or FEM calculations. To illustrate this methodology, Figure 1 depicts the adjoint application range and limitations. The adjoint approach allows the approximation of a nonlinear relationship by linearizing the underlying partial differential equations with regard to a geometry variation of a baseline design. Adjoint methods can therefore be applied as long as the geometry variations are small enough to only exhibit a linear effect.

Mulloth et al. [4] apply the adjoint method to evaluate the aerodynamic performance limiting the range based on blade surface curvature. All previous mentioned publications focused on the aerodynamic side till now. Turbine design, however, is multidisciplinary incorporating aerodynamics, heat transfer and structural mechanics. A tolerance design assessment, hence, needs to include also these multidisciplinary aspects.

Compared to the aerodynamic impact of manufacturing imperfections, the publications on the effect of manufacturing variations on blade life time are fairly limited. A FEM parameter study by Voigt et al. [5] investigates the effect of scatter in material and boundary parameters on thermo mechanical fatigue (TMF) life time. A recent publication by Hoegner et al. [6] evaluated the impact of manufacturing imperfections on turbine creep life time using 3D scan and computed tomography measurement data combined with a FEM Monte Carlo approach.

While aerodynamic adjoint solvers are widely available, structural adjoint solvers with life time objectives have only been recently developed. Gottschalk et al. [7] introduce a mechanical adjoint FEM solver to compute the probabilistic low cycle fatigue life time of a compressor blisk and optimize the blade geometry. In this publication, a similar approach has now been implemented into an in-house FEM solver using a hand-derived algorithmic adjoint approach to compute probabilistic low cycle fatigue (LCF) surface sensitivities. As an additional benefit

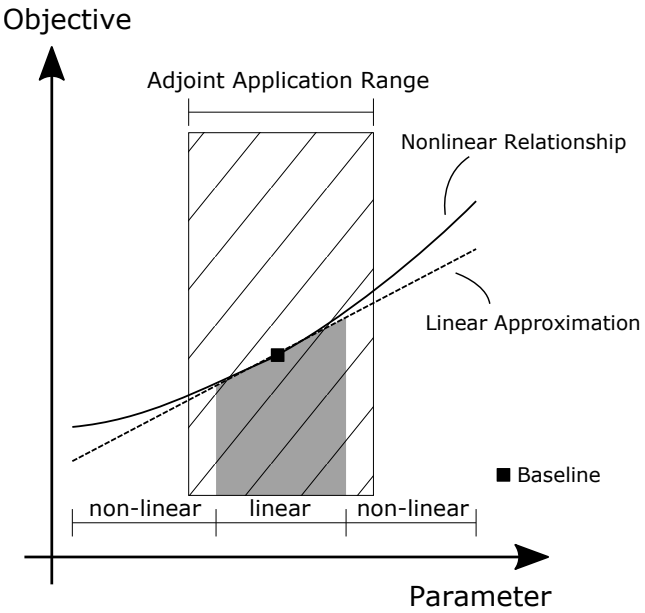

FIGURE 1: Adjoint Linear Approximation Example for a Parameter Variation

the application of the probabilistic LCF objective also provides a global life time functional, compared to multiple single evaluations points.

The aim of this paper is to show that CFD and FEM adjoint methods can be used to replace geometric with objective-based tolerances. The paper is structured in the following four parts: At first the adjoint probabilistic LCF method is introduced, including the derivation of the adjoint equations. The second part describes the analysis and the magnitude of the manufacturing imperfections of 102 turbine vane scans. In the third part the adjoint FEM and CFD solvers are validated using the 102 scans. The last part introduces the multidisciplinary adjoint based tolerance assessment tool chain, analyzing the adjoint surface sensitivities and quantifying the impact of manufacturing imperfections, as well as providing an outlook regarding the current imperfection model fidelity.

COMPUTATIONAL METHODS

Probabilistic LCF

Low cycle fatigue (LCF) denotes the life reduction of a turbine blade caused by cyclic loading, that can be, for instance, a consequence of start/stop cycles of an engine. The cyclic variation in the component strain leads to a first crack initiation, followed by the crack growth and final component failure. One turbine fatigue life time objective is therefore the number of cycles until a first crack on the component appears. For the analysis of fatigue crack initiation of surface driven LCF the relationship between strain ε and number of cycles N_i until crack initiation can be described by the Coffin-Manson-Basquin (CMB) equation as defined in Eq. 1.

$$\varepsilon = \frac{\sigma_f'}{E}(2N_i)^b + \varepsilon_f'(2N_i)^c, \tag{1}$$

see Rösler et al. [8] and Schmitz et al. [9] for more details. In the following N_i is also denoted as fatigue life. The first term of the CMB equation describes the fatigue behavior under linear-elastic deformation of the material, while the second term considers the case of plastic deformation. The coefficients $\sigma_f', \varepsilon_f', b, c, E$ are material parameters derived from material testing calibration methodologies such as maximum likelihood estimation. Note that additional crack growth assessments are not always needed in a design process and it would increase the mathematical complexity of the adjoint methodology significantly. Thus, such assessments will not be considered further in this work.

For the analysis of fatigue life, the two different approaches of deterministic and probabilistic design are now outlined. The deterministic LCF approach uses the CMB equations directly in combination with safety factors to account for the scatter of the material parameters and other uncertainties (safe-life approach), while the probabilistic LCF approach, that is considered in this work, applies a Weibull distribution $F_N(n)$, see Eq. 2.

$$F_N(n) = 1 - exp\left[-\left(\frac{n}{\eta_{LCF}}\right)^m\right], \tag{2}$$

The distribution explicitly considers the inherent scatter in fatigue life due to observed fatigue life variation in material tests which is a consequence of locally varying material properties. The Weibull shape parameter m is a material parameter that describes the inherent scatter. In order to also account for the statistical size effect, the Weibull scale parameter η_{LCF} integrates the CMB equations via a surface integral as defined in Eq. 3.

$$\eta_{LCF} = \left(\int_{\delta\Omega} \frac{1}{N_i^m} dA\right)^{-\frac{1}{m}}. \tag{3}$$

The CMB material parameters have different interpretation for the probabilistic approach and are in particular geometry independent in contrast to the deterministic CMB approach. All material data used for this work is Siemens AG proprietary data and was partly used in previous studies such as in Maede et al. [10].

To give an example of how to interpret the results of the probabilistic LCF method, Fig. 2 shows an exemplary cumulative Weibull distributions for the value $\eta_{LCF} = 10,000$ with three different Weibull shape parameters. The Weibull scale parameter η_{LCF} is also the 63% probability that crack initiation will appear on the blade surface after 10,0000 cycles. Note that this does not

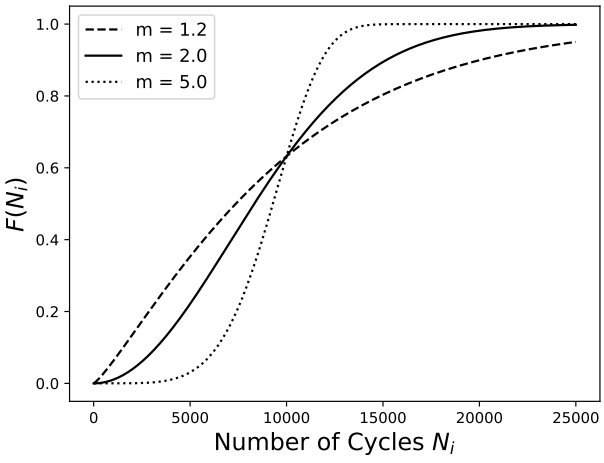

FIGURE 2: Example Cumulative Distribution with three Weibull Shape Parameters

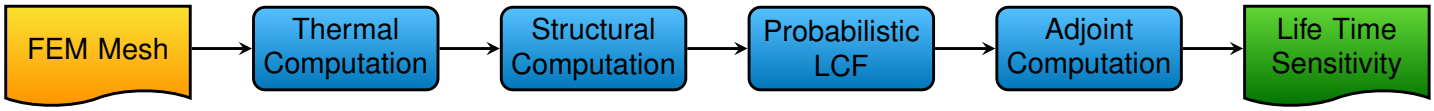

FIGURE 3: Adjoint Probabilistic Low Cycle Fatigue Sensitivity Analysis Steps

mean that the component will fail after 10,000 cycles, but that a first crack initiation has appeared. The general blade design evaluation process would be now to analyze the crack growth with fracture mechanics. The influence of the Weibull shape parameter, i.e. the material scatter of the test data, can be seen in the figure as a shift in the cumulative probability distribution $F(N_i)$.

A further advantage, compared to the deterministic safe life approach, is also that the probabilistic LCF approach provides with η_{LCF} a differentiable objective function, which can be used for the adjoint method in the next section.

Adjoint Probabilistic LCF

The objective function J used for adjoint probabilistic LCF approach is the Weibull scale parameter

$$J = J(u(X), X) = \eta_{LCF} \tag{4}$$

which depends on the surface node location X and the node displacement field $u(X)$. To evaluate the impact of surface geometry variations, we need to differentiate the objective J in regard to a surface node movement in normal direction x_i

$$\frac{dJ}{dx_i} = \frac{\partial J}{\partial u}\frac{du}{dx_i} + \frac{\partial J}{\partial x_i}. \tag{5}$$

In shape optimization, the underlying state equation is commonly seen as a constraint and the adjoint state which permits an efficient calculation of the shape sensitivities is the Lagrange multiplier, see e.g. Sokolowski et al. [11]. The same approach is adopted and applied to the the discretized finite element method equation for linear elasticity

$$K\bar{u} = \bar{f} \tag{6}$$

with the stiffness matrix K, the node displacement vector $\bar{u}$ and the right hand side term $\bar{f}$ representing the load vector consisting of thermal, pressure and structural loads. As a next step a Lagrange multiplier $\bar{\lambda}$ is introduced

$$L = J + \bar{\lambda}^T\left(\bar{f} - K\bar{u}\right). \tag{7}$$

For the derivation of L in regard to a node displacement x_i, the derivation results in

$$\frac{dL}{dx_i} = \frac{\partial J}{\partial x_i} + \frac{\partial J}{\partial u_j}\frac{du_j}{dx_i} + \bar{\lambda}^T\left(\frac{\partial \bar{f}}{\partial x_i} - \frac{\partial K}{\partial x_i}\bar{u} - K\frac{d\bar{u}}{dx_i}\right) \tag{8}$$

Next, the equation can be rearranged to highlight the more computational expensive terms, which results in

$$\frac{dL}{dx_i} = \frac{\partial J}{\partial x_i} + \bar{\lambda}^T\left(\frac{\partial \bar{f}}{\partial x_i} - \frac{\partial K}{\partial x_i}\bar{u}\right) + \left(\frac{\partial J}{\partial u_j} - \bar{\lambda}^T K\right)\frac{\partial \bar{u}}{\partial x_i}. \tag{9}$$

The partial derivatives of the first two terms on the right hand side are numerically easy to evaluate and the only main computational task would be to derive $\frac{\partial \bar{u}}{\partial x_i}$ because it depends on the evaluation of the FEM equations and the change in node displacement in regard to the surface node movement. However, if the bracket part of the last term of Eq. 9 becomes zero, the sensitivity of the probabilistic LCF model does no longer depend on $\frac{\partial \bar{u}}{\partial x_i}$. Therefore the bracket term is rearranged and solved for $\bar{\lambda}$ as shown in Eq. 10.

$$K^T\bar{\lambda}\left(\frac{\partial J}{\partial u_i}\right)^T = 0 \tag{10}$$

After solving for $\bar{\lambda}$, the Lagrangian derivative is reduced to the following:

$$\frac{dL}{dx_i} = \frac{\partial J}{\partial x_i} + \bar{\lambda}^T\left(\frac{\partial \bar{f}}{\partial x_i} - \frac{\partial K}{\partial x_i}\bar{u}\right) \tag{11}$$

The adjoint sensitivity of the probabilistic LCF model thus depends only on the evaluation of partial derivatives, which are computationally easy to compute. The required partial derivatives for the adjoint problem in Eqn. 10 and 11 are given in Eqn. 12 and 13.

$$\frac{\partial J}{\partial x_i} = J^{m+1}\int_{\delta\Omega}\left(N^{-m-1}\frac{\partial N_i}{\partial \sigma_{VM}}\frac{\partial \sigma_{VM}}{\partial x_i} + N^{-m}\frac{\partial |S|}{\partial x_i}\right)dS \tag{12}$$

$$\frac{\partial J}{\partial u_i} = J^{m+1}\int_{\delta\Omega}\left(N^{-m-1}\frac{\partial N_i}{\partial \sigma_{VM}}\frac{\partial \sigma_{VM}}{\partial u_i}\right)dS \tag{13}$$

The adjoint solver uses a constant temperature field assumption, similar to the adjoint CFD constant eddy viscosity assumption. This means that the component temperature is assumed constant w.r.t to the original baseline node positions. For example, in case the component becomes thicker and the metal temperature distribution should vary due to the increased thickness, the adjoint solver uses the same temperature field from the baseline geometry. The presented adjoint solver is thus a discrete hand-derived mechanical FEM adjoint solver.

The evaluation steps to analyze the sensitivities of the probabilistic LCF approach of a component are shown in Fig. 3. At first a thermal analysis in conducted. This is followed by a structural analysis and the probabilistic low cycle fatigue post processing. The analysis concludes with an adjoint probabilistic LCF computation solving Eq. 10. The life time sensitivity for the node surface is then evaluated for which the partial derivatives are computed for each single node surface direction. The final results are probabilistic LCF life time node sensitivities w.r.t a surface normal movement.

MANUFACTURING IMPERFECTIONS

For the validation of the adjoint aerodynamic and probabilistic LCF solver, 102 optical vane scans of a heavy-duty gas turbine are analyzed, which are obtained via 3D optical white-light scanning. These are the same scans as previously used by Liefke et al. [12, 13] for the aerodynamic assessment of surface imperfection with a CFD adjoint solver.

The manufacturing imperfection analysis starts with two inputs: an optical scan of the manufactured blade, which stores the blade surface geometry in an STL file format and a 2D triangle finite element surface mesh file from the baseline geometry. The FEM surface mesh is used in this context to reduce the number of surface points necessary to describe the manufacturing imperfection, while also providing the capability to limit the analysis process to specific regions such as the blade surface.

To compensate for the different Cartesian origin between FEM mesh and STL mesh, both meshes are overlapped by applying a translational shift of the coordinate origin of the STL file. Next, the distance between each FEM node and STL surface mesh is determined. This is achieved by computing the distance in normal direction between FEM node and STL mesh. The distance to the STL surface mesh is thereby determined through a ray casting. Additionally, to adjust for inlay errors from the blade scans, a six-point optimization, for a translational and rotational shift, is carried out for each blade scan to minimize the node distance between scan and 2D FEM mesh. The final results are, hence, 102 FEM surface offsets, which can be used for a quantification analysis and further processing such as mesh morphing.

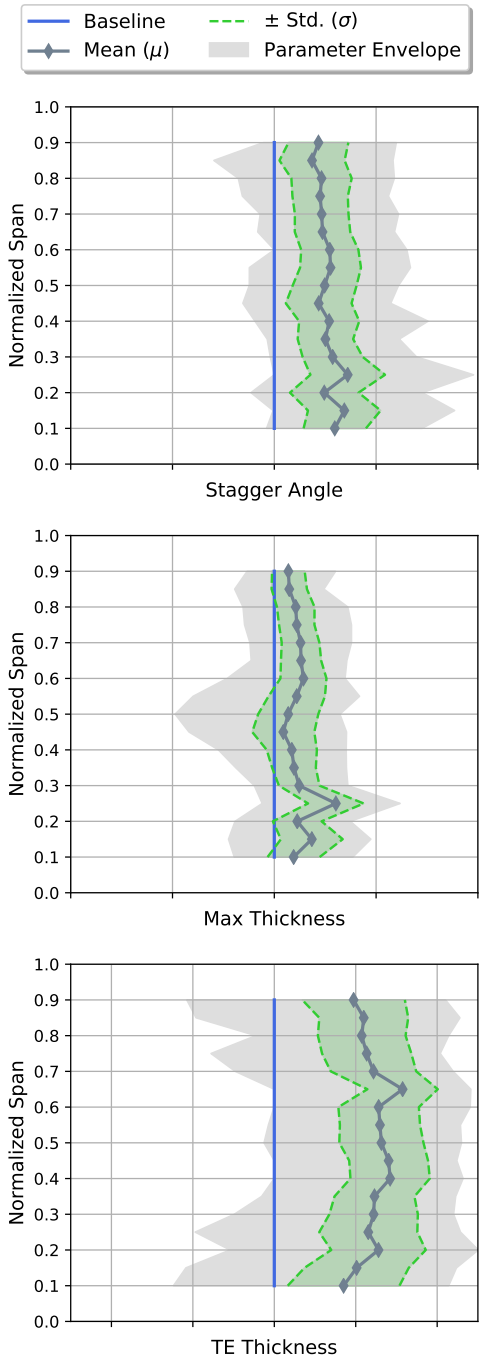

FIGURE 4: Section Normalized Manufacturing Imperfections

Parameter-based Quantification

The adjoint validation in the next section will apply the 102 deformed FEM and CGNS meshes directly without a previous separation into individual parameters.

In order to describe the magnitude of the manufacturing imperfections a NACA-like parameterization is applied. Thus, each

scan is divided into 17 sections between 10% and 90% blade span, excluding the areas of the vane fillet at hub and shroud. Fig. 4 shows the manufacturing imperfections quantification results for the 102 turbine vane scans for the parameters stagger angle, maximum thickness and trailing edge (TE) thickness. For data protection reasons each section value is normalized using the corresponding sections baseline value and only the arithmetic mean (μ) and standard deviation (σ) values are shown. Additionally, the parameter envelope is depicted as a gray area, showing the minimal and maximal value of each parameter.

The stagger and maximum blade thickness along the chord is slightly above the baseline thickness. Near 50% blade span the thickness parameter envelope shows a high reduction in max thickness, indicating that at least one blade was thinner than the baseline geometry. For the TE thickness the mean thickness is clearly above the baseline TE, highlighting that for a majority of blade scans the TE has been manufactured too thick.

ADJOINT VALIDATION LCF

Setup LCF

For the validation of the gradients computed by the adjoint method, 102 thermo mechanical FEM computations are conducted using deformed meshes. To quantify the difference between adjoint gradients and finite differences (FD) gradients, the absolute error is calculated according to Eq. 14.

$$\frac{\Delta F_{FiniteDifference} - \Delta F_{Adjoint}}{F_{Nonlinear}} \cdot 100 \;\; with \;\; F \;\; \in \{\eta_{LCF}, \eta_{is}\} \quad (14)$$

The nonlinear FD gradients are computed according to Eq. 15 using the baseline and a deformed mesh geometry, while the adjoint gradients are computed according to Eq. 16.

Because the implemented adjoint solver assumes a frozen temperature field, the validation is conducted with frozen and variable temperature field. This allows further to quantify the impact on the temperature field distribution due to surface imperfections.

The FEM application case is a heavy-duty turbine vane made of polycrystalline cast super alloy. The model consists of tetrahedral C3D4 elements and the computation is carried out for a thermo mechanical load case at its operating point. Additionally, the setup further includes thermal barrier coating (TBC) and bond coating (BC). After the thermal and structural analysis, the probabilistic LCF post processing is performed followed by solving the adjoint equations from Eq. 10.

$$\Delta F_{Nonlinear} = F_{Baseline} - F_{Deformed} \quad (15)$$

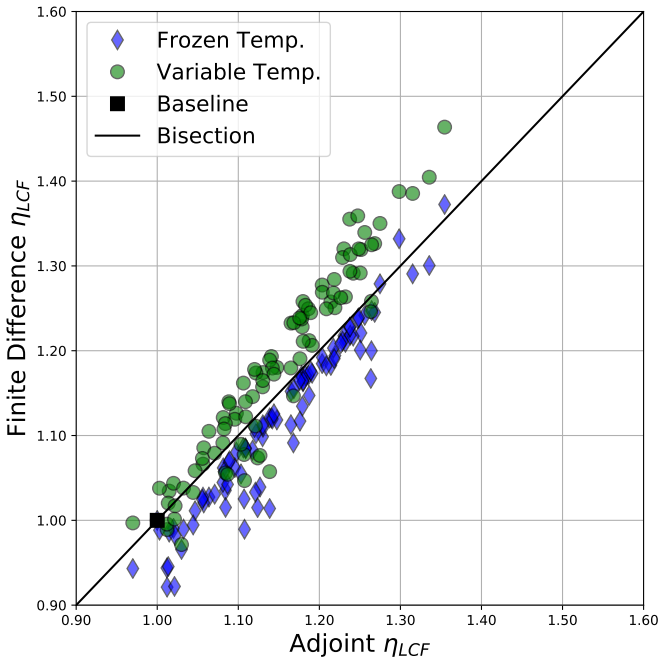

FIGURE 5: FEM Adjoint Gradients Versus Finite Difference Gradients for Probabilistic LCF Life Time

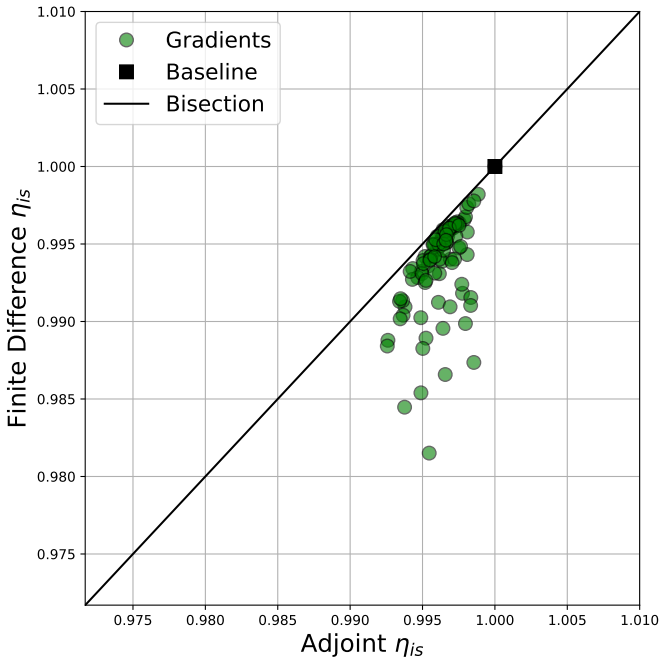

FIGURE 6: CFD Adjoint Gradients Versus Finite Difference Gradients for Isentropic Efficiency

$$\Delta F_{Adjoint} = \sum_{i}^{X} \frac{\partial J}{\partial x_i} \cdot \Delta x_i \tag{16}$$

The probabilistic LCF surface sensitivities are computed by moving all surface nodes individually in normal direction using Eq. 4. Furthermore, the probabilistic LCF integral is limited to the vane surface area for which the manufacturing imperfection are applied.

Results LCF

Fig. 5 displays the adjoint versus finite difference gradients of the Weibull scale parameter for all 102 scans. The results are plotted with frozen and variable temperature field finite differences, while the adjoint gradients remain identical. Thus, the finite difference values are shifted on the y-axis. The correlation coefficient between frozen finite difference and adjoint is 0.9623, while the coefficient is 0.9594 for the unfrozen finite differences. This proves that the surface imperfection impact is sufficiently linear and inside the range where adjoint can be applied.

The impact of manufacturing imperfection on blade life time can be seen to increase the average probabilistic LCF life time by around 12%. This is caused by the increased blade thickness observed in the previous sections, originating from a reduction in thermal strain due to an improved temperature distribution inside the component.

The absolute error of the Weibull scale parameter is shown in Fig. 7. Illustrating that the adjoint gradients overestimate the impact on the probabilistic LCF life time objective by around -2.5% compared to frozen finite differences. Compared to the variable temperature field FD gradients, adjoint probabilistic LCF is underestimated by +4.0%. For both cases the adjoint accuracy for over 90% of all scans is inside the range of ±5%.

Regarding the influence of the frozen temperature field, it can be seen that the variable temperature leads to a higher predicted probabilistic LCF life time of around 7.5%. This can be explained by the increased thickness of the blades. Considering that the main driver for low cycle fatigue are thermal strain gradients, the increased component thickness leads to a reduced thermal strain. Thus, the probabilistic LCF life time increases with an variable temperature field. It should be noted that component internal wall thickness variation has not been modeled and therefore the difference between frozen and variable finite differences might be lower than 7.5%.

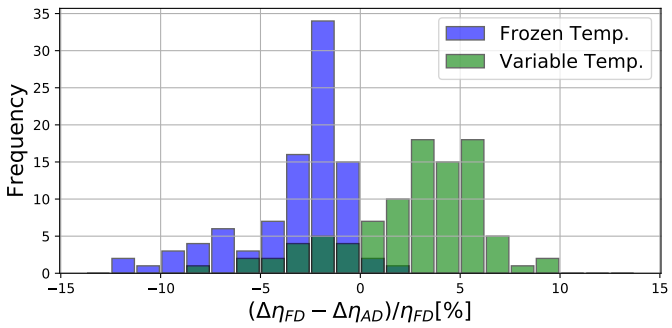

FIGURE 7: Weibull Scale Parameter Absolute Error for Frozen and Variable Temperature Finite Differences

ADJOINT VALIDATION CFD

Setup CFD

The analyzed 102 turbine vane scans are now used for a CFD adjoint gradient validation. As an objective the isentropic efficiency is used, which is defined in Eq. 17 using the total enthalpy H at the inlet and outlet of a turbine stage.

$$\eta_{is} = \frac{H_{02} - H_{01}}{H_{02,is} - H_{01}} \tag{17}$$

In order to quantify the aerodynamic isentropic efficiency, the CFD validation test case includes beside the vane also the following rotor blade. The rotor geometry remains according to the baseline design intent, while the vane geometries are replaced with 102 morphed CGNS mesh files.

The CFD computations are performed by applying the CFD solver TRACE and adjointTRACE, which is developed by the German Aerospace Center (DLR). Adjoint Trace is a discrete algorithmic derived adjoint flow solver, which is based on reverse mode differentiation of the primal CFD solver as shown by Backhaus et al. [14]. The mentioned CGNS mesh morphing is performed by using TRACE PREP, the pre-processor of TRACE, using an elliptic mesh deformation algorithm by Voigt et al. [15].

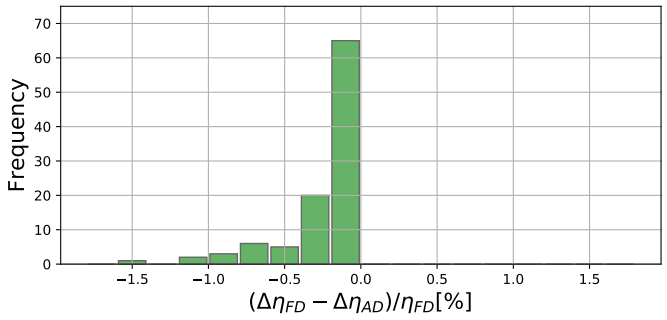

FIGURE 8: Isentropic Efficiency Absolute Error for CFD Adjoint Gradients

TABLE 1: Overview Computational Efficiency for Impact Quantification With Adjoint Probabilistic LCF vs Finite Differences

Description	Number	CPU Factor	Total
Baseline	1	1.00	1.00
Baseline + Adjoint Prob. LCF	1	1.33	1.33
Adjoint Multiplication	102	0.14	14.09
Frozen FD	102	0.82	83.58
Variable FD	102	1.00	102
Adjoint Impact Analysis			15.47
FD Impact Analysis			103

TABLE 2: Overview Computational Efficiency for Impact Quantification With CFD Adjoint Gradients vs Finite Differences

Description	Number	CPU Factor	Total
Primal CFD	1	1.00	1.00
Adjoint CFD	1	13.70	13.70
Adjoint Impact Analysis			14.70
FD Impact Analysis			103

Results CFD

Fig. 6 shows the adjoint versus finite difference gradients of the isentropic efficiency for the scanned 102 turbine vanes. It can be seen that the computed isentropic stage efficiency for all 102 scans is lower compared to the baseline design and that the adjoint gradients slightly overestimate the isentropic efficiency.

The absolute error of the CFD adjoint gradients is displayed in Fig. 8 and is calculated according to Eq. 14. For over 95% of all blade scans the absolute error between adjoint and finite difference gradients is below -0.5%.

It can be seen that around 10% of all blade scans show a higher absolute deviation compared to finite differences. While these deviations underline a non-linear effect, the adjoint method correctly evaluates the sign and general magnitude of the manufacturing imperfections with a maximum absolute error of 1.5%. The analyzed manufacturing imperfections are, hence, still inside the aerodynamic adjoint application range.

Computational Efficiency

Tab. 1 shows an overview of the computational cost of adjoint probabilistic LCF. Due to proprietary reasons only a CPU factor is given to compare the individual steps. The baseline computational time includes the FEM setup, the thermal computation, the structural computation and the probabilistic LCF post processing. The Adjoint probabilistic LCF step, hence, only requires 33% additional computational time compared to a sole baseline computation of the test case.

Also shown is the required computational time for the adjoint multiplication with a total factor of 0.14. This step includes the mesh morphing, the adjoint multiplication with shape sensitivities as well as data handling operations. The finite difference validation results consume for the frozen validation part 18% less time considering that no thermal computation step is necessary. In total the impact analysis with the adjoint requires only around 15% the time of the finite difference approach and is almost seven times faster.

Tab. 2 displays an overview of the computational efficiency of applying the adjoint CFD solver. One adjoint computation requires around 14 times the time of a primal CFD computation. Compared to a previous publication by Liefke et al. [12], this factor is higher, because the primal computation required a residual reduction below 10^{-6}. To achieve this level of convergence for an industrial test case the CFL number is continuously reduced to 1. For the comparison of adjoint and finite difference impact analysis the adjoint CFD approach also requires only 15% of the time. It should be noted that the adjoint multiplication time for the CFD impact analysis is below a CPU factor of below 0.01 and is thus not listed as part of the impact analysis.

TOLERANCE ASSESSMENT

Multidisciplinary tolerance assessment allows to define specific limits for aerodynamic and life time objectives. Thereby, providing the opportunity to effectively determine and limit the turbine component scatter. Point-based geometric tolerances prevent such a design capability and make it for the designer more difficult to decide between the main drivers of turbine blade manufacturing such as performance, manufacturability and product cost.

For the effective evaluation of objective-based tolerance bands instead of geometric tolerances, each manufactured blade needs to be analyzed. Fig. 9 shows a diagram of an analysis tool chain to quantify the impact on the blade life time and aerodynamic performance.

The analysis can be split in five individual steps:

1. Surface Imperfection Analysis
2. FEM Surface Node Movement
3. FEM Life Time Impact Evaluation
4. CFD Mesh Morphing
5. CFD Aerodynamic Impact Evaluation

The first surface imperfection analysis step is identical to the

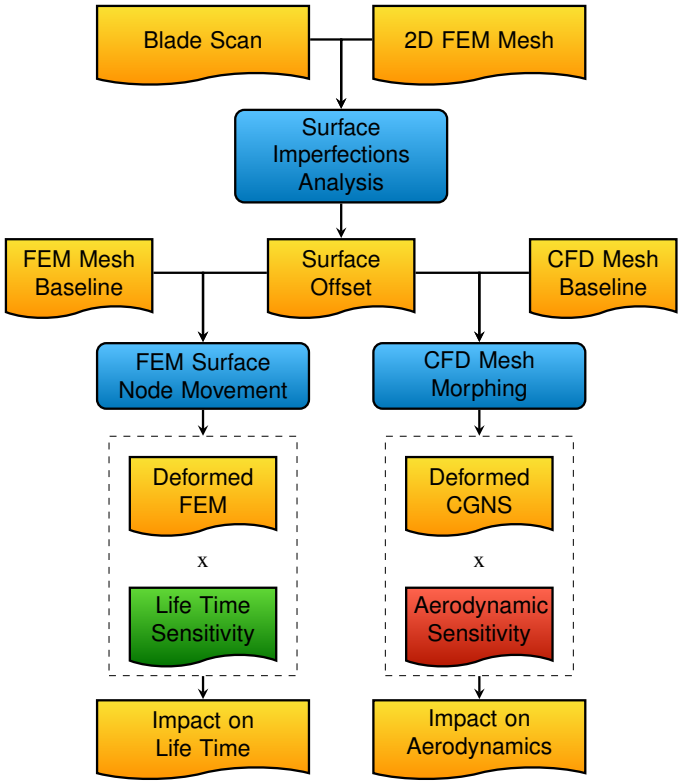

FIGURE 9: Multidisciplinary Impact Analysis Tool Chain

previously described manufacturing imperfection analysis in the second section of this paper. For the FEM surface node movement the baseline 3D FEM mesh surface nodes are moved in normal direction according to the computed 2D surface offset, producing 102 different FEM meshes of the analyzed turbine vane. Next, these 102 deformed FEM meshes can be evaluated by multiplying the deformation with the probabilistic LCF life time sensitivity, which is computed according to the process steps detailed Fig. 3.

For the aerodynamic analysis the surface offset points are handed over to a CGNS mesh morphing tool, which requires a bilinear interpolation to adjust for varying meshes between FEM and CFD baseline mesh. The CGNS mesh morphing step further requires a cold to hot transformation, assuming the aerodynamic simulation is done under hot loading conditions. Next, the generated deformed CGNS mesh files are used to be multiplied by the aerodynamic sensitivity surface field to quantify the aerodynamic impact of the manufacturing imperfections.

In the next section the adjoint surface sensitivities are analyzed to highlight the vane surface regions with the highest impact on isentropic efficiency and probabilistic LCF life time. Afterwards, the multidisciplinary scatter is quantified and an overview of the current imperfection modeling fidelity is presented.

Adjoint Surface Sensitivities

Fig. 10 displays the adjoint surface sensitivities for isentropic efficiency and probabilistic LCF life time plotted as a two-dimensional projection of span vs chord length for suction and pressure side of the turbine vane. The red areas indicate that a surface outward movement would increase the objective, while the blue areas indicate that a surface outward movement would decrease the objective.

For the isentropic efficiency objective three positive sensitivity areas (red) exist located at zone A, B and C on the vane suction side. These areas overlap with the position of a passage shock and an increase in curvature would reduce the shock losses and thus increase efficiency. The main negative area with zone F, is an area below Mach one and increasing the curvature would lead to an acceleration above Mach one with an increase in losses. On the pressure side near the TE a similar behavior can be observed for zone D and E, where an increase in curvature near a high Mach number would further increase losses.

The most sensitive regions for probabilistic LCF life time are located near the pressure side TE at zone G and H, while the remaining blade surface is insensitive. The high sensitivity near the fillet region can be explained by the increased Von Mises stresses near the fillet, which overlap with a thermal strain near a TE cooling feature. An additional outward movement of the fillet would thus reduce the stress near the fillet and also reduce the local thermal strain.

Impact of Manufacturing Imperfections

Fig. 11 shows a scatter plot for the isentropic efficiency and probabilistic LCF life time regarding the impact of the 102 turbine vane scans. The impact on probabilistic life time has been previously discussed showing a mean increased life of around 12%. The isentropic efficiency on the other hand shows a mean shift of around -0.4% stage efficiency due to the vane surface imperfections. The figure further depicts an exemplary tolerance range between 0.99 and 1.002 for isentropic efficiency and 0.95 and 1.3 for probabilistic LCF life time. Thereby, rejecting four blades out of the 102 scans.

Regarding the general trend of the impact of manufacturing variations it can be observed that the increased blade thickness, especially near the vane TE, leads to an increased blade life time. The aerodynamic efficiency, however, reduces due to the increased stagger angle and blade thickness. The tolerance assessment with adjoint provides, thus, sufficient information for objective-based tolerance assessment of turbine blades and vanes, proving that an intermediate decoupling step with geometric tolerances is no longer required. The analysis of the 102 vane scans shows further that the magnitude of the manufacturing imperfections are inside the adjoint application range and that the effect on aerodynamics and life time is sufficiently linear.

Other publications regarding the aerodynamic effect of man-

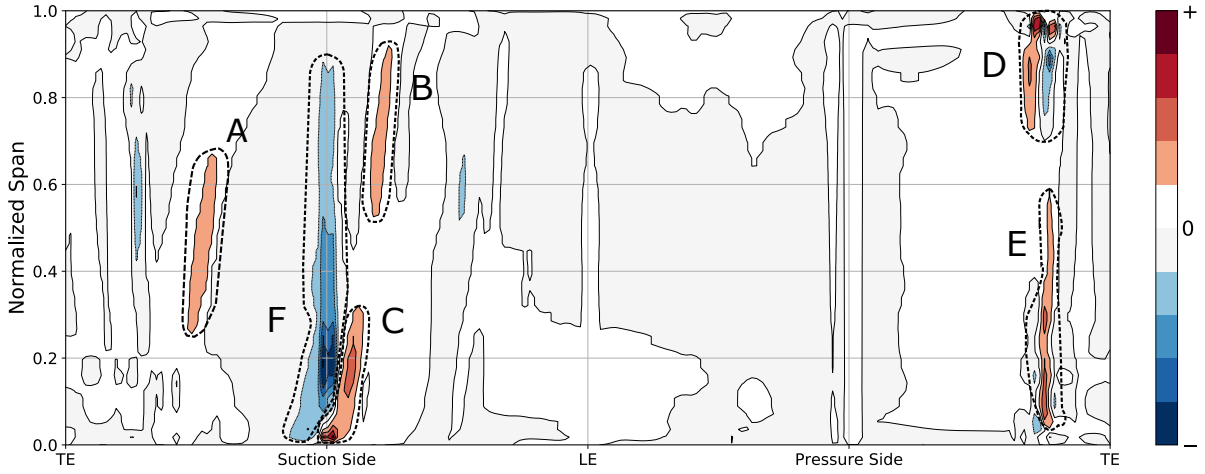

(a) Isentropic Efficiency Sensitivity

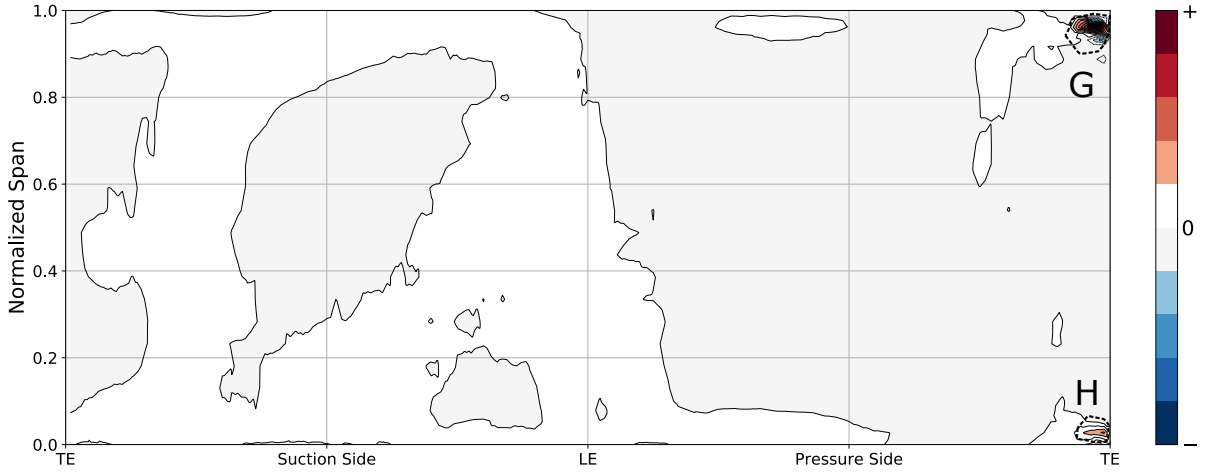

(b) Probabilistic LCF Sensitivity

FIGURE 10: 2d-Surface Projection Ranging From Leading Edge (LE) to Trailing Edge (TE). Red/Blue Color Indicates That a Surface Outward Movement Would Increase/Decrease the Objective

ufacturing imperfections show a similar trend of linearity for a majority of the investigated imperfections of turbine blades [16–18].

Towards Multidisciplinary Tolerance Design

The results presented prove that multidisciplinary tolerance assessment is possible using adjoint methods. However, the applied manufacturing surface imperfections only represent one aspect of a variety of possible sources for manufacturing imperfections. Fig. 12 therefore provides an overview regarding other sources, not yet included, in the current modeling of manufacturing imperfections.

This work has focused on external blade surface imperfections. Additionally, also end wall, tip clearance and wall thickness imperfections could be included. Another area, which the current modeling has neglected, are cooling imperfections. A variation in TBC and BC thickness, as well as film cooling hole shape and size variation would impact the cooling of the blade and thus the blade life time. Furthermore, internal cooling features such as pins and channel passage geometry also will impact the cooling flow and, hence, the blade life time. A detailed overview of the impact of cooling geometry manufacturing imperfections has been previously presented by Bunker [19], distinguishing between the varying magnitudes of impact.

A third area of imperfections are assembly imperfections. The blade assembly along the blade row might lead to a variation

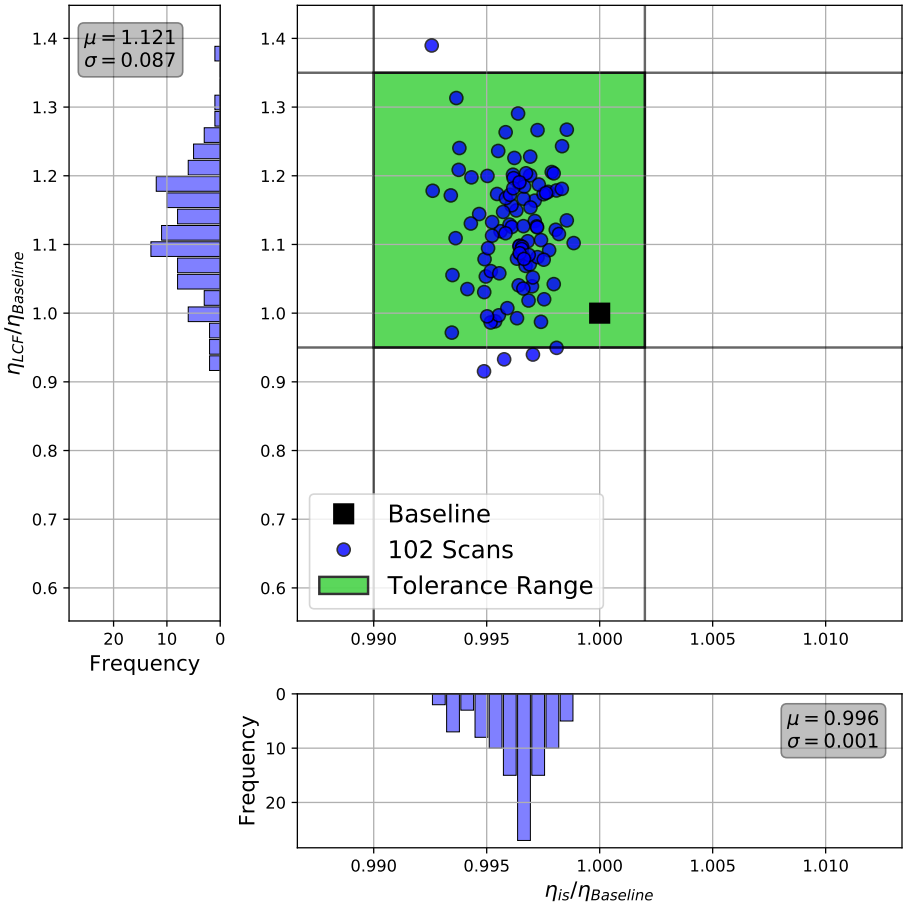

FIGURE 11: Manufacturing Imperfection Scatter of Baseline Normalized Isentropic Efficiency (η_{is}) vs Probabilistic LCF Life Time (η_{lcf}) Including Performance Tolerance Range

in the passage throat area and impact the blade passage interactions. In case of an applied re-staggering, especially for front turbine stages, this re-stagger should also be included. Furthermore, interplatform steps between blade passages could also impact the aerodynamic performance as shown in a study of Grewe et al. [20].

Another area are material imperfections. The probabilistic life time approach in this paper does not cover micro-structural imperfections, which also effect the life time as shown by Engels et al. [21]. Variations in the blade specific density are also not included and might be of importance regarding high cycle fatigue analysis or the mistuning of blades.

As shown, the accuracy of manufacturing imperfection modeling can be further increased by considering additional imperfections. While the current approach completely focused on the individual consideration of aerodynamic and life time quantities, the joint modeling of aerodynamics, life time and heat transfer would improve the prediction accuracy even further.

CONCLUSION

A multidisciplinary adjoint tolerances assessment tool chain is introduced for the impact analysis of real turbine blade manufacturing imperfections. It is proposed to replace geometric turbine blade tolerances with objective-based tolerances, to effectively control the aerodynamic efficiency and low cycle fatigue life time scatter of manufactured blades. So far this has not been possible due to the high computational demand to evaluate the impact of each manufactured blade.

The multidisciplinary tool chain is applied for the analysis of 102 optical turbine vane scans, showing that the average stage efficiency drops by 0.4% and the average LCF life time increases by 12%. Furthermore, the required computational time is reduced by 85%. A numerical validation of the adjoint gradients with finite differences further proves that the absolute error of the adjoint method is shown to be small enough and that the magnitude of real manufacturing imperfections is inside the adjoint application range.

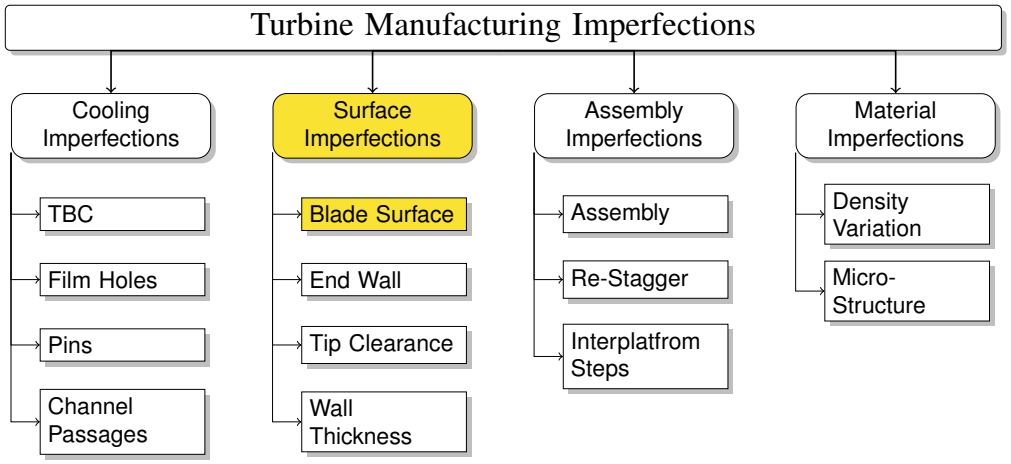

FIGURE 12: Overview Turbine Manufacturing Imperfections. Yellow Highlighted Imperfections Are Modeled as Part of This Paper

The absolute error for adjoint CFD gradients is below 0.5% and below 5% for LCF life time gradients. Hence, before the adjoint method can be applied, enough confidence in the approach needs to be gained by validating the adjoint application range with real manufacturing imperfections. The adjoint FEM accuracy could be further improved by applying a thermo mechanical adjoint solver, instead of the current mechanical adjoint solver.

The presented adjoint-based approach, however, is not the only possible way to analyze the impact of manufacturing imperfections. The application of other non adjoint-based methods such as surrogate models (Kriging, Radial basis functions, etc) therefore also seems possible, especially for non-robust blade designs.

The shown multidisciplinary approach combines isentropic efficiency and probabilistic low cycle fatigue life time for the tolerance assessment of blade surface imperfections. To increase the fidelity and accuracy of the tolerance assessment further, other sources of manufacturing imperfections, such as cooling or assembly, should be included. Furthermore, extending the number of aerodynamic and life time objective functions, would ultimately pave the way for a real digital twin for each manufactured blade.

ACKNOWLEDGMENT

The permission of Siemens Energy to publish the results is greatly acknowledged.

A. Liefke and H. Gottschalk acknowledge partial financial support from the GIVEN project, grant no. 05M18PXA "Mathematics for Innovation" by the Federal Ministry of Education and Research (BMBF).

REFERENCES

[1] Liu, J.-S., Zhu, D. X., Lew, B., and Rodriguez, A. D., 2018. "Aerodynamic and mechanical analyses on manufacturing variations of a turbine blade row". *ASME Turbo Expo 2018: Turbine Technical Conference and Exposition*.

[2] Dow, E. A., and Wang, Q., 2015. "The implications of tolerance optimization on compressor blade design". *Journal of Turbomachinery*.

[3] Nigro, R., Wunsch, D., Coussement, G., and Hirsch, C., 2017. "Uncertainty quantification in internal flows". In 55th AIAA Aerospace Sciences Meeting.

[4] Mulloth, A., Banks, G., Zamboni, G., and Bather, S., 2018. "A high fidelity quality assessment of high pressure turbine blades using surface curvature and gradient–based adjoint". *ASME Turbo Expo 2018: Turbine Technical Conference and Exposition*.

[5] Voigt, M., Mücke, R., Vogeler, K., and Oevermann, M., 2004. "Probabilistic lifetime analysis for turbine blades based on a combined direct monte carlo and response surface approach". *ASME Turbo Expo 2004: Turbine Technical Conference and Exposition*.

[6] Högner, L., Voigt, M., Mailach, R., Meyer, M., and Gerstberger, U., 2019. "Probabilistic fe-analysis of cooled high pressure turbine blades: Part b — probabilistic analysis". In ASME Turbo Expo 2019: Turbomachinery Technical Conference and Exposition.

[7] Gottschalk, H., Saadi, M., Doganay, O. T., Klamroth, K., and Schmitz, S., 2018. "Adjoint method to calculate the shape gradients of failure probabilities for turbomachinery components". In ASME Turbo Expo 2018: Turbomachinery Technical Conference and Exposition.

[8] Rösler, J., Harders, H., and Bäker, M., 2012. *Mechanical Behavior of Materials*, 4 ed. Springer Vieweg.

[9] Schmitz, S., Seibel, S. T., Beck, T., Rollmann, G., Krause, R., and Gottschalk, H., 2013. "A Probabilistic Model for LCF". *Computational Materials Science*.

[10] Mäde, L., Gottschalk, H., Schmitz, S., Beck, T., and Rollmann, G., 2017. "Probabilistic lcf risk evaluation of a turbine vane by combined size effect and notch support modeling". *ASME Turbo Expo 2017: Turbine Technical Conference and Exposition*.

[11] Sokolowski, J., and Zolésio, J.-P., 1992. "Introduction to shape optimization". In *Introduction to Shape Optimization*. Springer, pp. 5–12.

[12] Liefke, A., Marciniak, V., Janoske, U., and Gottschalk, H., 2018. "Using adjoint cfd to quantify the impact of manufacturing variations on a heavy duty turbine vane". In 7th European Conference on Computational Fluid Dynamics (ECCOMAS CFD 2018).

[13] Liefke, A., Marciniak, V., Backhaus, J., Frey, C., Gottschalk, H., and Janoske, U., 2019. "Aerodynamic impact of manufacturing variation on a nonaxisymmetric multi-passage turbine stage with adjoint cfd". In ASME Turbo Expo 2019: Turbomachinery Technical Conference and Exposition.

[14] Backhaus, J., Schmitz, A., Frey, C., Mann, S., Nagel, M., Sagebaum, M., and Gauger, N. R., 2017. "Application of an algorithmically differentiated turbomachinery flow solver to the optimization of a fan stage". In 18th AIAA/ISSMO Multidisciplinary Analysis and Optimization Conference.

[15] Voigt, C., Frey, C., and Kersken, H., 2010. "Development of a generic surface mapping algorithm for fluid-structure-interaction simulations in turbomachinery". In 5th European Conference on Computational Fluid Dynamics (ECCOMAS CFD 2010).

[16] Lee, W. Y., Dawes, W. N., Coull, J. D., and Goenaga, F., 2019. "The impact of manufacturing variability on multi-passage high pressure turbine aerodynamics". In AIAA Scitech 2019 Forum, p. 1950.

[17] Scharfenstein, J., Heinze, K., Voigt, M., Vogeler, K., and Meyer, M., 2013. "Probabilistic cfd analysis of high pressure turbine blades considering real geometric effects". In ASME Turbo Expo 2013: Turbine Technical Conference and Exposition, American Society of Mechanical Engineers.

[18] Brown, J. M., Beck, J., Kaszynski, A., and Clark, J., 2018. "Surrogate modeling of manufacturing variation effects on unsteady interactions in a transonic turbine". *ASME Turbo Expo 2018: Turbine Technical Conference and Exposition*.

[19] Bunker, R. S., 2009. "The effects of manufacturing tolerances on gas turbine cooling". *Journal of Turbomachinery*.

[20] Grewe, R. P., Miller, R. J., and Hodson, H. P., 2014. "The effect of endwall manufacturing variations on turbine performance". In ASME Turbo Expo 2014: Turbine Technical Conference and Exposition.

[21] Engel, B., Mäde, L., Lion, P., Moch, N., Gottschalk, H., and Beck, T., 2019. "Probabilistic modeling of slip system-based shear stresses and fatigue behavior of coarse-grained ni-base superalloy considering local grain anisotropy and grain orientation". *Multidisciplinary Digital Publishing Institute: Metals*.